Relaxation Processes in Nonlinear Optical Polyimide Side-Chain Polymers

Philip Kaatz,[†] Philippe Prêtre,[‡] Urs Meier, Urs Stalder, Christian Bosshard, and Peter Günter*

Nonlinear Optics Laboratory, Institute of Quantum Electronics, Swiss Federal Institute of Technology, ETH Hönggerberg, CH-8093 Zürich, Switzerland

Beat Zysset, Markus Stähelin,[§] Markus Ahlheim, and Friedel Lehr

SANDOZ Optoelectronics Research, SANDOZ Huningue SA, F-68330 Huningue, France

Received July 11, 1995; Revised Manuscript Received November 14, 1995[⊗]

ABSTRACT: Relaxation processes in nonlinear optical modified polyimide polymers with side-chain azo chromophores having glass transition temperatures in the range of $140 < T_g < 170$ °C have been studied. The relaxational mechanisms of the side-chain chromophores in these polymers have been investigated above and below the glass transition by second-harmonic decay, dielectric relaxation, and differential scanning calorimetry measurements. The *nonexponential* relaxation in both the time and frequency domains was modeled by the Kohlrausch−Williams−Watts (KWW) function. The *nonlinear* relaxational behavior of these polymers can be modeled in terms of the Tool−Narayanaswamy description of glassy state behavior. It allows for the nonlinear extension of the liquid equilibrium state behavior into and below the glass transition region with an accurate prediction of the relaxation times over more than 15 orders of magnitude in time. Time−temperature scaling of the relaxation times with $(T_g - T)/T$ as the relevant scaling parameter is observed below the glass transition.

I. Introduction

Understanding relaxational processes in nonlinear optical (NLO) polymeric materials is of critical importance in order to evaluate the long-term stability of poled polymers that are in development for potential electro-optic applications. Although the possibility of using poled polymers for nonlinear optical and electro-optic (EO) applications was proposed some time ago,[1,2] the actual usefulness of these materials has remained questionable due to stability problems of the poling-induced order of the NLO chromophores within these polymers. Previous work has demonstrated, however, that the basic concepts in developing poled polymers as NLO materials are well understood. The procedures employed in creating these oriented polymers are essentially as follows: an NLO-active chromophore is first incorporated into a polymer matrix (guest−host, side-chain, main-chain, and network matrices are typical examples). Heating the system at high temperature under an applied electric field results in the formation of an NLO-active medium due to the coupling of the polar chromophores to the electric field and the increased mobility of the liquid-like high-temperature phase of the polymer matrix. Cooling in the presence of the applied electric field gives a quasi-stable oriented system due to the formation of a polymer glass at lower temperatures. In general, amorphous polymers are preferred due to their superior optical properties. It is also preferable that the precursor polymer used for the NLO matrix has only primary or α-relaxation processes associated with the primary glass transition phenomena in order to minimize relaxation at low temperatures.

An essential requirement for stabilizing polymeric NLO materials is the formation of a glassy state at relatively high temperatures. Amorphous polymers, among other glasses, typically show evidence of a phase transition from a liquid-like to a glassy state when cooled from high temperatures. The temperature at which this transition occurs, known as the glass transition, T_g, is recognized to be primarily a kinetic phenomenon, whether or not it is valid to classify it as a true phase transition.[3] The physical origin of the glass transition is primarily associated with the cooperative motions of large-scale molecular segments of the polymer. The actual experimental observance of a glass transition, however, is most easily probed by measuring enthalpic changes in the polymer as a function of temperature via differential scanning calorimetry (DSC). Several phenomenological theories describe the primary aspects of the glass transition, at least as they are experimentally observed.

We make use of a variation of one of these phenomenological theories in an attempt to gain a better understanding of the temperature dependence of relaxational processes in NLO polymers. An algorithm has been developed that allows us to model most of the observed thermal responses of glassy polymers as they are probed by DSC measurements. The model then enables us to calculate relaxation times as a function of both temperature and processing conditions (cooling rates, annealing times and temperatures, etc.). We have also made corresponding relaxational measurements of the side-chain chromophores above T_g by dielectric relaxation and below T_g by decay of the second harmonic intensity produced from poled polymer films. The combination of these measurements gives insight into the nature of relaxation processes in NLO polymers and allows us to make a definitive assessment of comparative chromophore stability in a variety of NLO polymer matrices.

* To whom correspondence should be addressed. Phone: +41-1-633 22 95; Fax: +41-1-633 10 56.

[†] Current address: Department of Physics, University of Nevada, Las Vegas, Las Vegas, NV 89154.

[‡] Current address: Department of Electrical and Computer Engineering, University of California, Davis, CA 95616.

[§] Current address: Department of Physics, University of Basel, 4056 Basel, Switzerland.

[⊗] Abstract published in *Advance ACS Abstracts,* February 1, 1996.

0024-9297/96/2229-1666$12.00/0

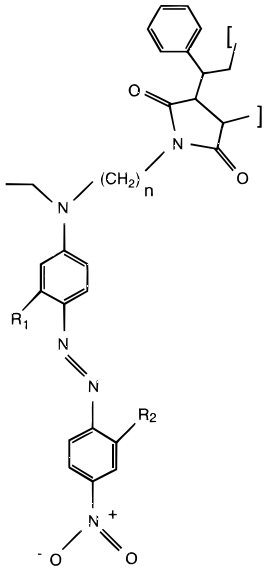

Figure 1. Chemical structures of the nonlinear optical side-chain polyimide polymers studied in this work.

Table 1. Nomenclature and Azo Dye Substitution Patterns for the Three Polymers Discussed in This Paper

polymer	*n*	R_1	R_2
A-095.11	3	CH_3	H
A-097.07	3	CH_3	Cl
A-148.02	2	H	H

II. Nonlinear Optical Polyimide Side-Chain Polymers

The chemical structures of the polymers studied in this work are shown in Figure 1. The alkylamino-functionalized NLO azo chromophores, with the various substitution patterns shown in Table 1, were attached via a two- or three-carbon spacer linkage to an alternating styrene−maleic−anhydride copolymer as reported elsewhere.[4] The three polymers denoted by A-095.11, A-097.07, and A-148.02 with the chromophores indicated in Table 1 were chosen for the relaxation measurements described in this work. In a previous communication, we have reported measurements characterizing the linear and nonlinear optical properties of these polymers.[5] In this work, we concentrate on characterizing the relaxational mechanisms in these NLO side-chain polymers.

III. Theoretical Discussion

When a liquid is subjected to a sudden change in temperature T, its physical properties such as volume V, viscosity η, or enthalpy H undergo an instantaneous, solid-like change followed by a slower, liquid-like relaxation to new equilibrium values at the new temperature. Remarkably, all classes of liquids (e.g. ionic, molecular, and polymeric) show the same qualitative behavior. It is generally presumed that this structural relaxation involves some change in the average molecular configuration of the liquid. The time $\Delta t'$ required for the relaxation increases rapidly with decreasing temperature. The liquid is said to enter the *glass transition region* when its time scale $\Delta t'$ and the time scale Δt of an observer are of the same order of magnitude. *Above* the glass transition region ($\Delta t' \ll \Delta t$), the structure rearranges promptly in response to changes in T, and measured properties are said to be those of an equilibrium liquid. *Below* the glass transition region ($\Delta t' \gg \Delta t$), structural rearrangements are kinetically arrested. They do not contribute to changes in measured properties in response to changes in temperature, and the material is referred to as a glass.

Relaxation processes to the equilibrium state in polymeric and other glassy materials are known to be highly nonlinear and nonexponential:[6] nonlinear in the sense that the rate of relaxation depends on the magnitude and direction of the temperature jump, and nonexponential because the relaxation function cannot accurately be described by a single exponential decay function.

(a) Modeling Structural Relaxation in Polymeric Glasses. A variety of theoretical expressions exist that describe the temperature dependence of relaxation processes in polymeric materials time based on free volume, entropy or other phenomenological expressions.[3,7,8] In general, these phenomenological models do not provide a method of *ab initio* calculation of glassy-state behavior and properties, but they are able to provide a good representation of volumetric and enthalpic relaxation and recovery processes. A common feature of all of these expressions is a partitioning of the relaxation time into an Arrhenius temperature dependent part and a term describing the temperature dependence of the structural, or configurational relaxation of the polymer molecules. The structural relaxation time of polymeric liquids, as interpreted by Di Marzio and Gibbs,[9] involves the cooperative rearrangement of a number of molecular segments of the polymer molecule. Adam and Gibbs[10] subsequently obtained an expression for the structural relaxation time in terms of the configurational entropy S_c of the relaxing molecular segments which can be written as

$$\tau = A \exp\left(\frac{E}{kTS_c}\right) \tag{3.1}$$

where $E = \Delta\mu S_c^*$ is an activation energy, k is Boltzmann's constant, and T is the temperature. The potential barrier for a rearrangement is given by $\Delta\mu$, and S_c^* is the corresponding configurational entropy of the smallest group of molecules that undergo a rearrangement. S_c is the configurational entropy of the glass due to the kinetic formation of a nonequilibrium state. Scherer[11] has presented arguments that it can be calculated from

$$S_c = \int_{T_2}^{T_f} \frac{\Delta C_p}{T}\, dT \tag{3.2}$$

where $\Delta C_p = C_{pe} - C_{pg}$ is the isobaric heat capacity difference of the liquid equilibrium and the glassy states, respectively. We assume that the temperature T_2 in this formulation is equivalent to the "Kauzmann temperature",[12] T_K, which is described by $S_c = 0$. Within the concept of a fictive temperature, originally proposed by Tool,[13] T_f is defined as the temperature at which the observed enthalpy would attain an equilibrium value. In terms of enthalpic parameters, it can be defined as

$$T_f = T + \frac{H - H_e}{\Delta C_p} \tag{3.3}$$

or equivalently,

$$H(T) = H_e(T_f) - \int_T^{T_f} C_{pg}\, dT' \tag{3.4}$$

where $H_e(T_f)$ is the equilibrium value of the enthalpy at the fictive temperature T_f. In terms of eqs 3.3 and

3.4, the fictive temperature describes the relaxational part of the enthalpy expressed in temperature units. It allows for the introduction of *nonlinearity* in the description of structural relaxations. Differentiation of eq 3.4 shows that the isobaric temperature coefficient of T_f at temperature T,

$$\frac{dT_f}{dT} = \frac{C_p(T) - C_{pg}(T)}{C_{pe}(T_f) - C_{pg}(T_f)} \approx \frac{C_p(T) - C_{pg}(T)}{C_{pe}(T) - C_{pg}(T)} \quad (3.5)$$

is the relaxational part of the heat capacity normalized to zero for the glassy state and to unity for the equilibrium liquid. On the right-hand side of eq 3.5, it is assumed that $\Delta C_p(T_f) \approx \Delta C_p(T)$, which is a good approximation in the transition region.[7]

Narayanaswamy[14] has given an explicit procedure, which will be denoted the TN (Tool−Narayanaswamy) analysis, for the quantitative calculation of the fictive temperature based on an assumption of thermorheological simplicity. Further details for incorporating *nonexponentiality* in this procedure have been provided by Moynihan et al.,[15,16] by making use of the KWW function (see below; this function provides a convenient description of relaxation processes, but not one that is necessary from theoretical considerations) in describing the enthalpic relaxation and recovery process. Using this procedure, the value of T_f can be calculated from the previous thermal history by using the following expression:

$$T_f = T_0 + \int_{T_0}^{T} dT' \left\{1 - \exp\left[-\left(\int_{T'}^{T} \frac{dT''}{q\tau}\right)^b\right]\right\} \quad (3.6)$$

where $q = dT/dt$ is the heating/cooling rate and T_0 is an arbitrary reference temperature above the glass transition temperature.

The calculation of the relaxation time τ can be achieved with the use of eqs 3.1 and 3.2. Assuming that ΔC_p is inversely proportional to the temperature, Hodge has shown that the following expression can be derived for the relaxation time associated with the cooperative chain rearrangements:[17,18]

$$\tau = A \exp\left(\frac{B}{T(1 - T_2/T_f)}\right) \quad (3.7)$$

where BR is an activation energy with R the gas constant, T is the temperature, and A is a time parameter. The assumption that the heat capacity is hyperbolic is not essential for the description of glass transition behavior, but it does greatly facilitate the interpretation of the parameters A, B, and T_2 in terms of other phenomenological theories as will be further discussed below. Several other functional relationships of the relaxation time τ have also been considered,[17−20] but the results have usually been found to be inferior to those obtained with the use of eq 3.7.

(b) Relaxation Functions. A useful functional representation for describing a variety of nonexponential relaxational mechanisms in polymers in the time domain is the stretched exponential or Kohlrausch−Williams−Watts[21,22] (KWW) function, which can be written as

$$\phi(t) = \exp[-(t/\tau)^b] \quad (3.8)$$

with $0 < b \leq 1$. More generally, a nonexponential relaxation function $\phi(t)$ can conveniently be considered as arising from a superposition of exponential relaxation functions (see, e.g., Beckmann[23] for a discussion of other commonly used relaxation functions). The continuous distribution of relaxation times $\rho(s)$ is sometimes approximated by a discrete distribution of single-exponential functions described by weighting factors g_i as

$$\phi(t) = \int_0^\infty \varrho(s) \exp[-(t/s)]\, ds \approx \sum_{i=1}^{n} g_i \exp[-(t/s_i)] \quad (3.9)$$

where normalization requires the integral over $\rho(s)$ or the sum over g_i to be equal to one. As relaxation usually proceeds over many time scales, the distribution is more typically described in terms of the logarithmic relaxation spectrum $G(\mu)$ with $\mu = s/\tau$. For the case of the KWW function, the distribution of relaxation times $G(\mu)$ can be written as[24]

$$G(\mu) = s\varrho(s) = -\frac{1}{\pi}\int_0^\infty \exp(-x) \exp[-(x\mu)^b \cos(\pi b)] \sin[(x\mu)^b \sin(\pi b)]\, dx \quad (3.10)$$

which has the series representation of [24,25]

$$G(\mu) = -\frac{1}{\pi}\sum_{n=0}^{\infty} (-\mu^b)^n \frac{\Gamma(bn+1)}{\Gamma(n+1)} \sin(nb\pi) \quad (3.11)$$

where Γ is the Gamma function. The normalized distribution of relaxation times for the KWW function with $b = 0.5$ and 0.25 are shown in Figure 2. For comparison, the distribution weights g_i obtained by Moynihan et al.[26] by optimizing a series expansion of discrete exponentials fitted to the KWW function as described by eq 3.9 are also indicated in the figure. In contrast to previous work, we do not find it necessary or advantageous to use a discrete distribution of exponential functions to approximate the KWW function for modeling either enthalpic[20,27−30] (DSC) or dielectric relaxation processes.[31−34]

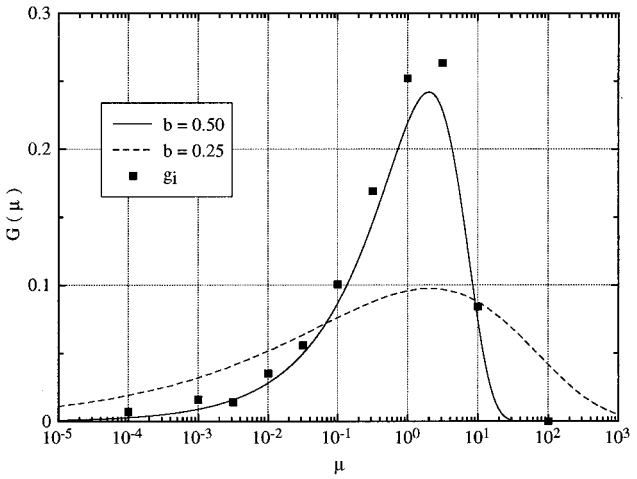

Figure 2. Normalized logarithmic distribution $G(\mu)$ of relaxation times of the Kohlrausch−Williams−Watts (KWW) function. If there was a single relaxation time, we would have a δ-function for $\mu = s/\tau = 1$. The points are from Moynihan et al.[26]

(c) Adam−Gibbs Parameter Correlations. Hodge[19] has noted that correlations exist between the Adam−Gibbs DSC parameters A, B, and T_2 used in eq 3.7 but indicated that theoretical developments of the prefactor A were not well developed. Using an algorithm based on eqs 3.5−3.7, we investigated the nature of the correlation between these three parameters. For the purpose of determining the glass transition tem-

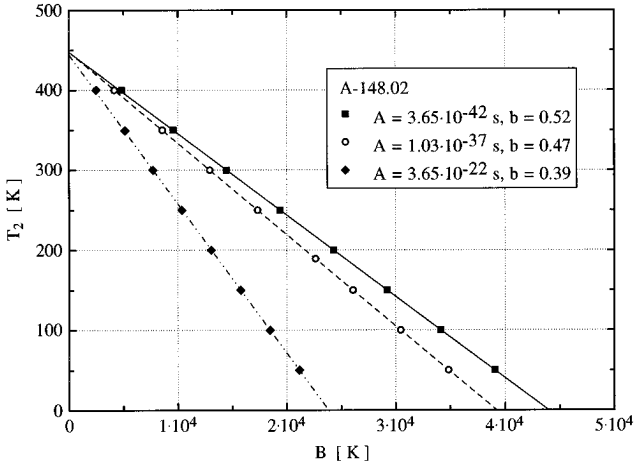

Figure 3. DSC parameters T_2 vs B of the polyimide side chain polymer A-148.02. Each point represents a parameter set where B was determined from a least squares fit to the measured data (see Figure 10) with fixed parameters A and b as indicated in the inset and also fixed T_2 value as given on the ordinate. Note that the intercepts are very close to the glass transition temperature.

perature, it is not necessary to consider the nonexponential parameter b. Calculations indicate that this parameter has a negligible effect on the glass transition temperature. The effect of b is primarily manifested in the nature of the thermal hysteresis observed on the heating portion of the DSC cycle. The other three parameters A, B, and T_2 were determined to be coupled together by some relation, given a specific polymer with a glass transition temperature T_g. Holding A and b constant, the value of T_2 was determined as a function of B from the DSC analysis of A-095.11 and A-148.02 as shown in Figure 3. See the discussion in section IVa and Figures 5, 10, and 11 for the data evaluation of DSC traces.

These results indicate that a linear relation exists between T_2 and B with an intercept very close to the corresponding value of T_g:

$$T_2 \approx T_g + f(A)B \tag{3.12}$$

The functional form *f(A)* becomes more obvious in a plot of A as a function of B (holding this time T_2 and b constant during the evaluation) as indicated in Figure 4a. Figure 4b shows corresponding DSC traces. These results show that B and *ln(A)* are also linearly coupled with a slope of $-1/(T_g - T_2)$ and an intercept τ_g, which corresponds to the relaxation time at T_g. Combining these observations with eq 3.12 yields the following functional form for *f(A)*:

$$1/f(A) = \ln(A/\tau_g) = -\frac{B}{T_g - T_2} \tag{3.13}$$

Combining the results of Figures 3 and 4a,b and eq 3.13 indicates that the following ratio, R_{AG}, of the Adam–Gibbs DSC parameters should be nearly constant for all glasses if τ_g is assumed to be indicative of the glass transition:

$$R_{AG} \equiv \frac{-\ln A\,(T_g - T_2)}{B} \tag{3.14}$$

Alternatively, making use of the relaxation time, τ_g, the preexponential factor A in eq 3.7 can be replaced by the expression

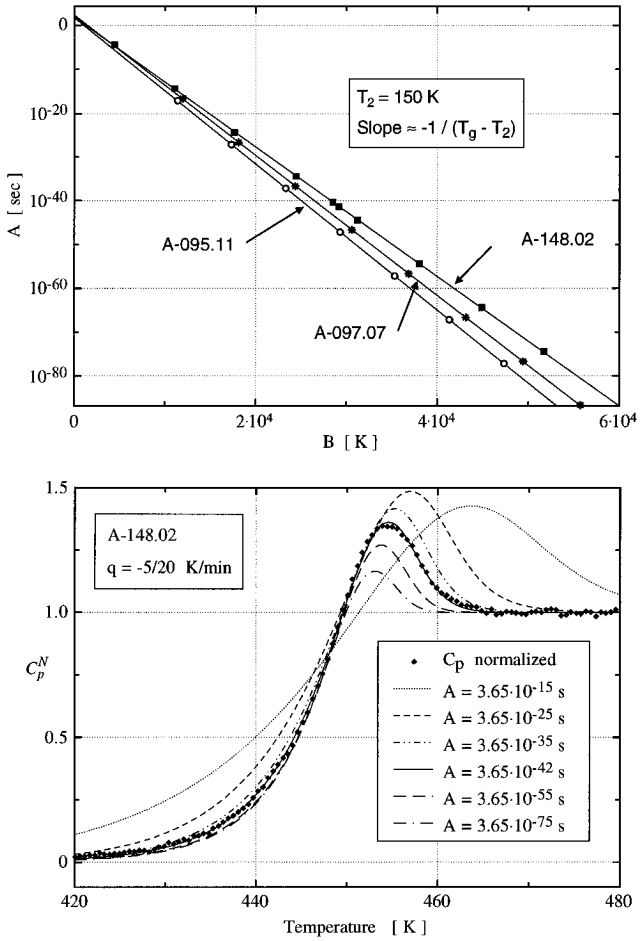

Figure 4. (a) DSC parameters A vs B of all the polyimide side-chain polymers in a semilogarithmic plot. The evaluation procedure is similar to the description in Figure 3: parameters T_2 (=150 K) and b held fixed and A fixed as given on the ordinate during the determination of B. The slope is calculated to be very close to $-1/(T_g - T_2)$. (b) DSC traces for the polyimide side-chain polymer A-148.02 as a function of the time factor A with T_2 (=150 K) and b (=0.52) fixed (see Figures 5, 10, and 11 for the data evaluation). Each curve has a corresponding point in (a).

$$A = \tau_g \exp\left(\frac{-B}{T_g - T_2}\right) \tag{3.15}$$

Gómez Ribelles et al.[35] have used an equivalent form of this relation by defining a reference temperature T_{ref} such that $\tau_{ref} = 1$ s. The identification of T_{ref} with T_g and τ_{ref} with τ_g, however, allows us to make a useful comparison of the TN formalism with the well-known Williams–Landel–Ferry (WLF) theory as will be further discussed below.

The results obtained from the current and previously analyzed DSC data are collected in Table 2.[7] We find the ratio R_{AG} to be slightly less than one for very different types of glasses. We have reanalyzed the DSC data of NBS 710,[11] B_2O_3,[20,36] and ZBLA[20,36] glasses, as the parameters published for these glasses give relaxation times τ_g (calculated via eq 3.15) that differ substantially from the others. Our results for these glasses give relaxation times τ_g at the glass transition of approximately 10–100 s, in agreement with the other glasses.

(d) Tool–Narayanaswamy (TN)/Williams–Landel–Ferry (WLF) Relations and Limiting Time–Temperature Behavior. The relaxation time at any temperature can be normalized with respect to the relaxation time at the glass transition temperature,

Table 2. Adam−Gibbs Parameters and Ratio R_{AG} for Previously Analyzed DSC Data Together with Best Fit Values for Our Polymers from Figure 4a

material	$-\ln(A/s)$	B (10^3 K)	T_2 (K)	T_g (K)	b	τ_g (s)	R_{AG}	ref[a]
A-095.11	108.7	29.3	150	410	0.44	54	0.96	TW
A-097.07	153.6	43.1	150	422	0.29	128	0.97	TW
A-148.02	95.42	29.2	150	444	0.52	42	0.97	TW
PVAc	66.60	6.23	225	313	0.55	66	0.94	19
PVC	59.74	2.61	320	361	0.28	51	0.94	19
PS	100.3	17.1	210	373	0.74	100	0.96	19
PS	63.5	7.63	260	373	0.54	56	0.94	19
PMMA	55.45	3.43	325	382	0.34	110	0.92	19
PC	70.30	7.03	325	420	0.54	40	0.95	19
glycerol	34.20	2.18	134	193	0.51	16	0.93	20
glycerol	43.41	3.37	120	193	0.51	16	0.94	20
NBS 710	32.83	8.06	494	845	0.63	5.2×10^{-5}	1.43	11
NBS 710	19.11	6.62	554	845	0.68	38	0.84	TW
NBS 711	34.95	18.9	248	730	0.67	71	0.89	36
B_2O_3	25.68	11.6	286	564	0.65	9.3×10^6	0.61	20, 36
B_2O_3	35.74	11.2	285	564	0.70	82	0.89	TW
P_2O_5	23.69	13.0	150	605	0.77	130	0.83	58
$Pb(PO_3)_2$	69.20	18.7	350	603	0.64	110	0.93	58
ZBLA	61.38	12.5	425	587	0.46	7.1×10^6	0.80	20, 36
ZBLA	59.45	10.3	425	587	0.54	52	0.94	TW

[a] TW = this work.

$R_\tau^g = \tau/\tau_g$. Combining this with eq 3.15 for the prefactor A and with eq 3.7 gives the following expression for the normalized relaxation time ratio R_τ^g:

$$R_\tau^g = \frac{\tau}{\tau_g} = \exp\left(-\frac{B}{T_g - T_2} + \frac{B}{T(1 - T_2/T_f)}\right) \quad (3.16)$$

Equation 3.16 provides a theoretical basis for discussing limiting relaxation behavior both above and below T_g.

Above the glass transition temperature, $T_f \approx T$, since the structure is in thermodynamic equilibrium, and the preceding expression reduces to the functional form of the Fulcher−Tammann−Hesse (FTH) equation,

$$R_\tau^g = \exp\left(-\frac{B}{T_g - T_2} + \frac{B}{T - T_2}\right) \quad (3.17)$$

At $T = T_g$ the right side of eq 3.17 equals 1 and one is indeed led to associate τ_g with the relaxation time at the glass transition temperature. Equation 3.17 is also easily related to the WLF equation, which is usually written as[6,37]

$$\log R_\tau^g = -\frac{C_1^g(T - T_g)}{C_2^g + (T - T_g)} = -C_1^g + \frac{C_1^g C_2^g}{T - T_2} \quad (3.18)$$

where B of the FTH equation is related to the WLF parameters by $B = 2.303 C_1^g C_2^g$. The temperature T_2 can be written as $T_2 = T_g - C_2^g$, with $C_2^g \approx 50$ °C if "universal" relaxational behavior (in the WLF sense) is assumed. More realistically, however, universal behavior is not valid and values of C_2^g from mechanical and dielectric measurements of glassy polymers above T_g vary over a considerable range from about 40 to 100 °C.[6] Using the WLF parameters, the previously defined Adam−Gibbs ratio (eq 3.14), R_{AG}, can be written as

$$R_{AG} = 1 - \frac{\log \tau_g}{C_1^g} \quad (3.19)$$

Taking values for τ_g and C_1^g of 10−100 s and 17, respectively, a ratio of $R_{AG} = 0.88-0.94$ is obtained, which is the range of R_{AG} for most of the glasses in Table 2.

It should be noted that there is no *a priori* reason for the TN or WLF parameters to have the same values when they are determined from different measurement procedures; e.g., the fictive temperatures describing enthalpic, volumetric, dielectric, mechanical, or other relaxation processes are most likely different.[15,16] However, it is commonly found that relaxation processes near the glass transition temperature scale similarly and therefore they are usually observed to have the same functional relationships.

Below the glass transition T_f reaches a final limiting value in simple cooling processes, i.e., without sub-T_g annealing. This final T_f, may be defined[38,39] to be the glass transition temperature; however, in practice it is more convenient to define T_g by some experimentally determined procedure, e.g., the midpoint definition of $C_p^N = 0.5$. For the case of simple cooling processes, however, the exact procedure of determining T_g is of little consequence as the results are all within a few degrees of each other; see section VIb. Assuming the final fictive temperature to be T_g, we obtain the following temperature dependence below T_g of the normalized relaxation time ratio:

$$R_\tau^g \approx \exp\left(\frac{B}{T_g - T_2}\frac{T_g - T}{T}\right) = \exp\left(2.303 C_1^g \frac{T_g - T}{T}\right) \quad (3.20)$$

This result indicates that the primary or α-relaxation processes should have an Arrhenius temperature dependence below the glass transition. In addition, from the "universality" of the WLF parameter C_1^g, one might expect normalized relaxation time ratios to scale with the scaling parameter $(T_g - T)/T$, at least in the same class of glass-forming liquids (e.g., polymers).

(e) Dielectric Relaxation. The measurement of the frequency dependence of the dielectric constant gives useful information on the relaxation of electric dipole moments in a polarizable medium, which are perturbed from their equilibrium configuration by an (oscillating) external electric field. The dielectric relaxation depends

on $\langle\cos\theta\rangle$, the orientational average of the cosine of the angle between the dipole moment of the molecule and the direction of the electric field, which is related to the dipole moment correlation function for the orientational motion of dipoles.[40−42] The normalized relaxation function $\phi(t)$ describing the correlation of the retarded decay of these dipole moments is in turn related to the frequency-dependent complex dielectric constant $\epsilon^*(\omega) = \epsilon'(\omega) - i\epsilon''(\omega)$ of the material by[43]

$$\frac{\epsilon^*(\omega) - \epsilon(\infty)}{\epsilon(0) - \epsilon(\infty)} = -\int_0^\infty \exp(-i\omega t)\,\frac{\mathrm{d}\phi(t)}{\mathrm{d}t}\,\mathrm{d}t \quad (3.21)$$

where $\epsilon(\infty)$ is the high-frequency limit and $\epsilon(0)$ is the dc dielectric constant. Assuming that the relaxation $\phi(t)$ can be described by the KWW function (eq 3.8) and inserting this into eq 3.21 gives

$$\frac{\epsilon^*(\omega) - \epsilon(\infty)}{\epsilon(0) - \epsilon(\infty)} = -\int_0^\infty \exp(-iuz)\,\mathrm{d}[\exp(-u^b)] \quad (3.22)$$

with $z = \omega\tau$ and $u = t/\tau$. Integrating by parts, this becomes

$$\frac{\epsilon^*(\omega) - \epsilon(\infty)}{\epsilon(0) - \epsilon(\infty)} = [1 - \pi z V(z)] - i\pi z Q(z) \quad (3.23)$$

where *Q(z)* and *V(z)* are the standard integrals:

$$Q(z) = \frac{1}{\pi}\int_0^\infty \exp(-u^b)\cos(zu)\,\mathrm{d}u \quad (3.24)$$

$$V(z) = \frac{1}{\pi}\int_0^\infty \exp(-u^b)\sin(zu)\,\mathrm{d}u \quad (3.25)$$

Series expansion of these integrals was first considered by Cauchy[44] with later important contributions by Wintner.[45] Subsequently, they have been discussed and/or rederived by others.[31−33,46−49] Two series expansions are needed for high and low frequencies due to the slow rate of convergence or possible divergence for different values of *b*. We use the expressions given by Williams et al.:[46]

$$zQ(z) = \frac{1}{\pi}\sum_{n=1}^{\infty}(-1)^{n-1}\frac{1}{z^{nb}}\frac{\Gamma(nb+1)}{\Gamma(n+1)}\sin\frac{nb\pi}{2} \quad (3.26a)$$

$$zV(z) = -\frac{1}{\pi}\sum_{n=0}^{\infty}(-1)^{n-1}\frac{1}{z_{nb}}\frac{\Gamma(nb+1)}{\Gamma(n+1)}\cos\frac{nb\pi}{2} \quad (3.26b)$$

and

$$zQ(z) = -\frac{1}{\pi}\sum_{n=1}^{\infty}(-1)^{n-1}\frac{z^{n-1}}{\Gamma(n)}\Gamma\left(\frac{n+b-1}{b}\right)\sin\frac{(n-1)\pi}{2} \quad (3.27a)$$

$$zV(z) = -\frac{1}{\pi}\sum_{n=0}^{\infty}(-1)^{n-1}\frac{z_n^{-1}}{\Gamma(n)}\Gamma\left(\frac{n+b-1}{b}\right)\cos\frac{(n-1)\pi}{2} \quad (3.27b)$$

These two series expressions have different regions of convergence for different values of *b*. In order to achieve a fast rate of convergence for arbitrary values of *b* with $0.05 < b < 0.95$, eqs 3.26 are used if $\log z > -P(b)$, where *P(b)* is determined empirically from

$$P(b) = 5.9198 - 25.492b + 160.41b^2 - 563.45b^3 + 940.22b^4 - 740.99b^5 + 223.55b^6 \quad (3.28)$$

otherwise eqs 3.27 are used.

(f) Analysis of the Decay of the SHG Intensity. Second-order nonlinear optical effects in NLO polymers require molecules with nonvanishing second-order microscopic polarizabilities and a macroscopic polar order. An external electric field provides the alignment of the chromophores by coupling to their dipole moments. This poling procedure imposes an ∞mm point group symmetry on the polymer. The susceptibility tensor for second harmonic generation, $\boldsymbol{d}(-2\omega;\omega,\omega)$, has only three independent elements for the ∞mm point group. If the Kleinman symmetry conditions are satisfied for SHG measurements sufficiently removed from optical resonance, the number of susceptibility tensor elements reduces to just two, d_{33} and d_{31}. One of them, d_{31}, is best suited for decay studies in such polymers, as it can be obtained directly from the experimental SHG measurements without the need of additional assumptions or measurements.[5]

For many molecules with strong optical nonlinearities along a single charge transfer axis *z* (donor−acceptor groups at the end of π-electron systems as in the azo chromophores used in this work), it is usually appropriate to assume that the component β_{zzz} of the hyperpolarizability tensor along this axis is large enough to describe the nonlinear optical properties in a first approximation. The relation between the macroscopic value of the second-order nonlinearity and the microscopic hyperpolarizability can then be written as:[50]

$$d_{31} = \frac{1}{2}N\beta^*_{zzz}\,\frac{1}{2}(\langle\cos\theta\rangle - \langle\cos^3\theta\rangle) \quad (3.29)$$

where the notation is the same as in section IIIe.

For moderate poling fields ($E_p \le 200$ V/μm), one can write

$$d_{31} \approx \frac{1}{30}\,\frac{N\beta^*_{zzz}\mu^*_{g,z}E_p}{kT} \quad (3.30)$$

where *N* is the number density of dye molecules, $\mu^*_{g,z}$ is the ground-state dipole moment along the *z*-axis, and *k* is the Boltzmann constant. The asterisk refers to local field corrected values due to the influence of neighboring molecules.

The time dependence of the SHG decay due to orientational relaxation ("*or*") of the NLO chromophores was found to be highly nonexponential and was in general well represented by a KWW function of the form

$$d^{or}_{31}(t) = d^{or}_{31}(0)\exp[-(t/\tau_{or})^b] \quad (3.31)$$

as was used previously to describe enthalpic (DSC) and dielectric relaxation processes.

(g) Comparison of Orientational Relaxation Times. In order to compare orientational relaxation times from different measurement techniques, relaxation functions such as eqs 3.21 and 3.31 should point to the same underlying decay mechanism. As mentioned above, dielectric relaxations depend on $\langle\cos\theta\rangle$. This seems at first to be in conflict with eq 3.29. In a study of transient properties of poled polymer films, Wu[51] indicated that the two terms in eq 3.29 exhibit a temporal decay with two characteristic time constants, the faster (by a factor of 6) associated with the decay of $\langle\cos^3\theta\rangle$. In addition, the amplitude for the fast decay is much smaller than that describing the $\langle\cos\theta\rangle$ decay.

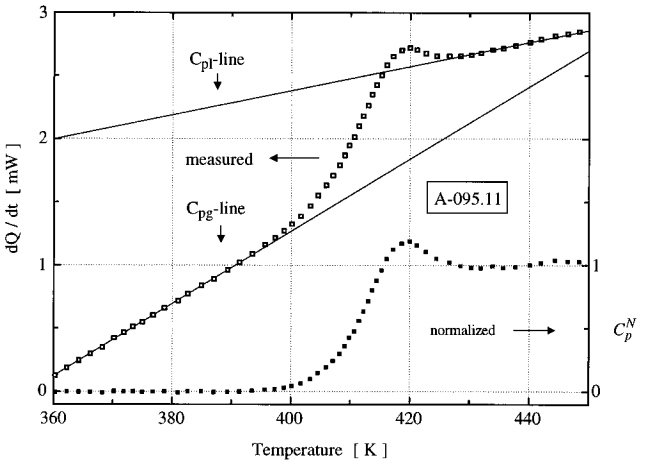

Figure 5. DSC normalization process.

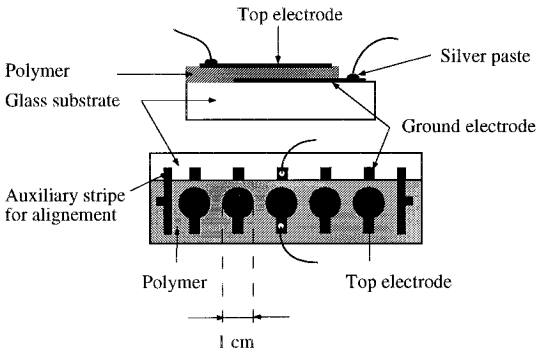

Figure 6. Electrode pattern used for the dielectric measurements. The films were cast on microscope slides. The auxiliary stripes on both sides were used for the alignment of the mask for evaporating the top gold electrode.

If therefore Wu's theory is applicable, one may conclude that dielectric and SHG decay measurements probe essentially the same relaxation processes.

IV. Experiments

(a) Differential Scanning Calorimetry (DSC) Measurements. DSC measurements were done with a commercial Perkin-Elmer DSC-2C apparatus. The samples were prepared as pressed powder capsules of about 15−30 mg. A typical measurement procedure was accomplished as follows: the polymer sample was first heated to an initial temperature of about $T_g + 50$ K for approximately 15 min. Subsequent cooling was done at a constant rate between −0.62 and −40 K/min to at least 60 K below T_g and then further reheated at a constant rate to the initial temperature. Data were collected on the heating portion of the cycle. The measured heat flow $dQ(T)/dt$ is related to the polymer heat capacity $C_p(T)$ by

$$\frac{dQ(T)}{dt} = m_p q C_p(T) \tag{4.1}$$

where m_p is the polymer mass and $q = dT/dt$ is the heating/cooling rate. The calculated heat capacity can be compared to the DSC measurement by defining the normalized heat capacity (cf. eq 3.5):

$$C_p^N(T) = \frac{dT_f}{dT} = \frac{C_p(T) - C_{pg}(T)}{C_{pe}(T) - C_{pg}(T)} \tag{4.2}$$

where C_{pg} and C_{pe} are the heat capacities in the glassy and equilibrium temperature regions sufficiently extrapolated from the relaxation temperature region, as indicated in Figure 5.

(b) Dielectric Measurements. A Hewlett-Packard HP 4129A LF impedance analyzer with a frequency range of 5 Hz to 13 MHz and a Zehnder IM5 impedance analyzer for frequencies down into the mHz regime were used for the dielectric measurements. The impedance measurements were done according to the "lumped circuit" method[40] in either a parallel or series configuration as indicated in Table 3.

Table 3. Lumped Circuit Configuration

	parallel	series
Configuration	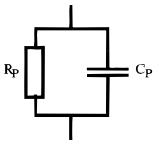	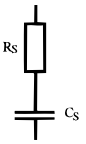
Complex Impedance	$\frac{1}{Z_P} = \frac{1}{R_P} + i\omega C_P$	$Z_S = R_S + \frac{1}{i\omega C_S}$
Real part of $\varepsilon^*(\omega)$	$\varepsilon' C_0 = C_P$	$\varepsilon' C_0 = \frac{C_S}{1+tan^2(\delta)}$
Imaginary part of $\varepsilon^*(\omega)$	$\varepsilon'' C_0 = \frac{1}{\omega R_P}$	$\varepsilon'' C_0 = \frac{\omega R_S C_S^2}{1+tan^2(\delta)}$
with	$C_0 = \frac{\varepsilon_0 A}{d}$	$tan(\delta) = \frac{\varepsilon''}{\varepsilon'} = R_s C_s \omega$

Films of each polymer with thicknesses ranging from 1 to 5 μm were spin cast from solutions (5:1) of cyclopentanone/*N*-methyl-2-pyrrolidone (NMP) of varying polymer concentration onto glass slides, which were coated with a gold bottom electrode pattern as seen in Figure 6. The films were partially removed and subsequently dried for 1 day at a temperature $\approx$ 170 °C. The top gold electrode was deposited in a way that the contacts did not overlap with the bottom electrode. Typical values for C_0 were in the range 0.1−0.7 nF (the electrode area was 0.79 cm^2, with film thicknesses between 1 and 5 μm).

All of the dielectric loss spectral measurements show a large rise at low frequencies. The large increase in ϵ'' is most likely due to the dc conductivity σ_0 of the polymer, which is usually described as follows:[52−54]

$$\epsilon''_{dc}(\omega) = \frac{\sigma_0}{\epsilon_0 \omega} \tag{4.3}$$

A common method of treating the dc conductivity of the samples is to fit it with a potential function of the form $a\omega^k$ with $k \approx -1$ and subtract it from the measured data. With high T_g polymers, however, this procedure is not suitable, since the ϵ'' loss peak merges with the dc conductivity in ϵ'' at low frequencies and is seen just as a shoulder rather than as a peak; see Figure 7. Instead, we use an analytical scheme developed by Howell et al.[52,54] By analogy to mechanical relaxation, an "electric modulus" M^* is defined, which may be termed a complex inverse permittivity:

$$M^*(\omega) \equiv 1/\epsilon^*(\omega) = (M_\infty - M_0)[1 - N^*(\omega)] + M_0 \tag{4.4}$$

where $N^*(\omega) = N'(\omega) - iN''(\omega)$ is given by an analogous expression to eq 3.21. M_∞ is the high and M_0 the low frequency limit of the real part of M^*. First, the imaginary part M'' was calculated from measured ϵ^* data and subsequently fitted according to eq 4.4. Second, the results for M'' together with the real part data M' from the first conversion were backconverted to yield corrected ϵ'' values. Finally, these ϵ'' values were again fitted to the Laplace transform of the KWW decay function. An illustration of this correction procedure is shown in Figure 7.

(c) Measurements of the Decay of the SHG Intensity. Relaxation of the side-chain chromophores below the glass transition was investigated by the decay of the SHG signal from either corona- or electrode-poled films. Films of each polymer with thicknesses ranging from 0.3 to 2.5 μm were spin cast from solutions of cyclopentanone/*N*-methylpyrrolidone (5:1) of varying polymer concentration onto ITO-coated glass substrates. For the electrode-poled films, a gold film was deposited onto the polymer film to provide a second electrode. The polymer films were baked at approximately 170 °C for 1 day to remove any residual solvent.

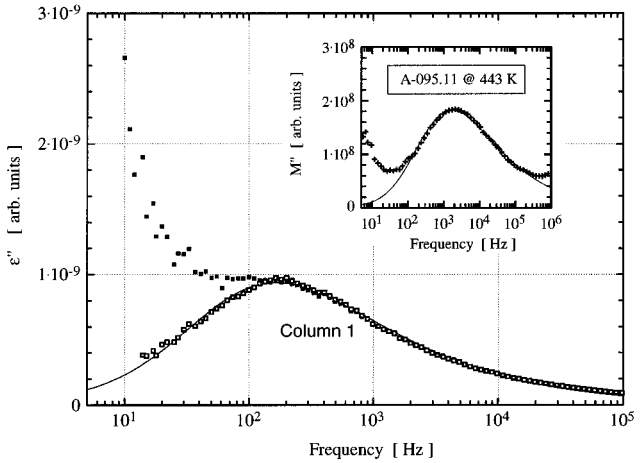

Figure 7. Correction procedure to obtain the dielectric loss relaxation times. The polymer conductivity prevents an accurate fit to ϵ''. Use of the electric modulus M″, however, allows the dielectric loss peak to be deconvolved from the dc conductivity (see inset). Filled squares indicate values obtained in the original measurement, while open squares are the results after the correction procedure.

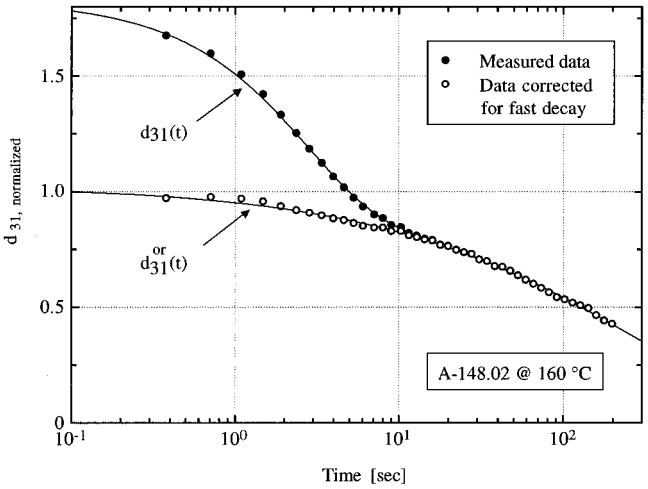

Figure 8. SHG relaxation of the polyimide side-chain polymer A-148.02 at 160 °C. The fast decay due to $\chi^{(3)}$ effects and the release of charge carriers is assumed to have an exponential time dependence. The orientational contribution of the NLO chromophores to the SHG signal is fitted to the Kohlrausch−Williams−Watts (KWW) function.

After poling slightly above the glass transition temperature, the polymer films were cooled with an applied poling field at a rate of ≈ 2−5 °C/min to the sample temperature at which the decay process was observed. This temperature was chosen to be in the range from 80 °C up to T_g for the individual polymers. Either a 30 Hz Q-switched Nd:YAG laser operating at 1338 nm or a 800 Hz Q-switched Nd:YLF laser operating at 1313 nm was used for the SHG decay experiments.

Corona-poled films: At the decay temperature the corona field was turned off and the SHG signal was continuously monitored for a time period of up to 100 h depending on the decay temperature. Data for the decay at 80 °C were measured in logarithmic time intervals over more than 1 year.

Electrode-poled films: At the decay temperature the electrodes were short-circuited and the SHG signal was continuously monitored for a time period of up to 100 h depending on the decay temperature.

In both cases, the SHG signal was detected with a PMT and a boxcar averager with 0.1−1 s integration time and active baseline subtraction. A quartz reference signal was monitored concurrently to reduce laser fluctuations and correct for possible drifts in the laser intensity level over the long acquisition times involved in the decay measurements.

All of the decay experiments exhibit a fast initial decay amounting to about 20−30% of the total initial SHG signal during the first few minutes. We attribute this decay to the electric field induced third-order effect [55,56] (γ) and to the release of charge carriers trapped in the film in the case of corona poling. In most cases the contribution from this fast decay has been isolated by introducing an extra single-exponential function for this initial decay in eq 3.31:

$$d_{31}(t) = [d_{31}(0) - d_{31}^{or}(0)] \exp[-(t/\tau_\gamma)] + d_{31}^{or}(0) \exp[-(t/\tau_{or})^b] \quad (4.5)$$

There is only one additional fit parameter, τ_γ, compared to eq 3.31, since $d_{31}(0)$ can directly be taken from the measurement. Typically, τ_γ is several orders of magnitude smaller than τ_{or} and has no influence on the value of the latter. The result of this procedure is demonstrated in Figure 8 for the case of the SHG decay of A-148.02 at 160 °C.

V. Results

(a) Stretched Exponent *b*. Although it is not possible to predict absolute values for the stretched exponent b in different experiments, one expects higher values ($b \approx 1$) far above T_g and a decrease in b (or a broadening of the relaxation spectrum) with decreasing temperature ($b \approx 0$ in the vicinity of T_2). Certainly, b is a smooth function of temperature, and therefore relaxation times from measurements with strongly fluctuating b values should not be compared with each other.

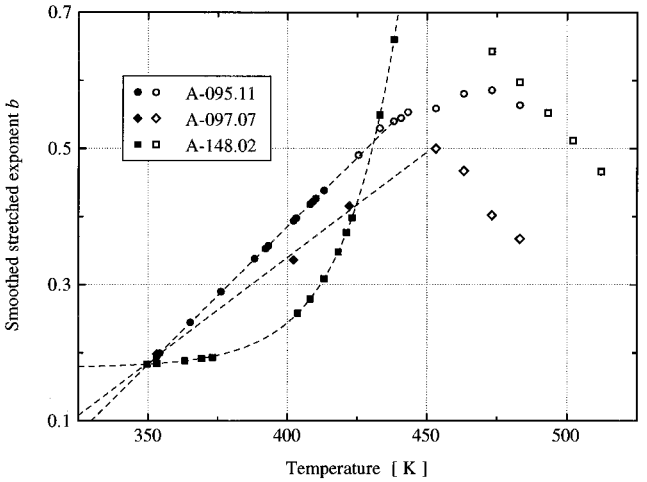

Figure 9. Assumed smooth temperature dependence of the Kohlrausch−Williams−Watts (KWW) parameters b of the NLO polymers. Filled points refer to SHG, open points to dielectric measurements.

Our procedure was as follows: first, we determined b independently from all SHG measurements. Best fit values for the stretched exponent for polymers A-095.11 and A-097.07 showed a linear temperature dependence below T_g. Stretched exponents for polymer A-148.02 showed a pronounced increase close to the glass transition. Dielectric data matched those from SHG relaxation near T_g with an unexpected systematic decrease for A-097.07 and A-148.02 at higher temperatures. Assuming a smooth temperature dependence as indicated in Figure 9, we evaluated all measured data a second time with b held fixed at each temperature. This procedure never changed the corresponding relaxation times by more than one-half an order of magnitude.

Hodge[18] proposed the following empirical form for the stretched exponent b from DSC measurements:

$$b \approx 1 - \frac{T_2}{T_f} \quad (5.1)$$

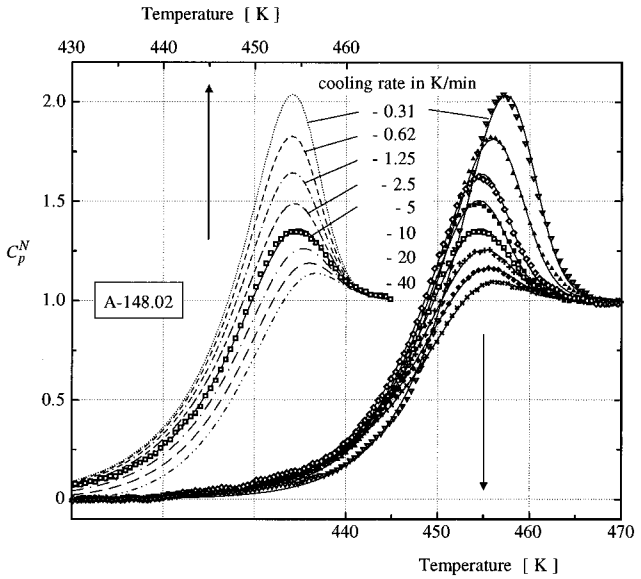

Figure 10. Normalized C_p^N DSC heat capacity curves of the polyimide side-chain polymer A-148.02 for different cooling rates as indicated in the figure. The heating rates were all at 20 K/min. The right side displays experimental results with best fits. The left side gives the theoretical expectation based on the parameter set of the trace with cooling rate 5 K/min.

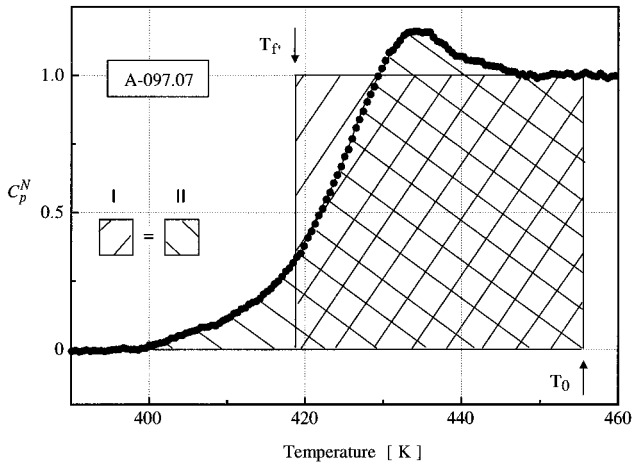

Figure 11. Graphic representation of the final fictive temperature $T_{f'}$ using the equal-area construction. The data are from the polymer A-097.07.

Table 4. Enthalpic Adam−Gibbs Parameters for the Polymers Investigated in This Work

polymer	B (10^4 K)	T_2 (K)	T_g (K)	b	log[τ_g(s)/s)]	R_{AG}
A-095.11	2.5 ± 0.4	160 ± 20	410	0.45 ± 0.04	1.7 ± 1.0	0.96
A-097.07	6 ± 2	160 ± 20	422	0.25 ± 0.06	2.5 ± 0.8	0.97
A-148.02	2.7 ± 0.5	170 ± 40	444	0.50 ± 0.03	1.2 ± 0.6	0.97

This expression is the simplest form for which b tends to 1 for high temperatures and to 0 for temperatures close to T_2. We found b to be about 10−30% lower than this prediction, as has been previously observed for most polymers.[7]

(b) Differential Scanning Calorimetry (DSC). An extensive set of DSC traces for A-148.02 is shown in Figure 10. Data were collected on the heating portion of the thermal cycle as a function of cooling rate and with a constant heating rate of 20 K/min. The curves with the lowest cooling rates were taken at the end of the series. The shift in peak temperature might be due to chemical degradation of the chromophores, since the same sample was used for the series of DSC measurements. Theoretical expectations based on the parameter set with $q = -5/20$ K/min are displayed on the left side. As seen in Figure 10, the calculated peak height and peak position are in good agreement with the experimental results. However, the overall peak shape demands different parameter sets to obtain best fits. The parameters for the overall best fits shown in Figure 10 are given in Table 4.

One possible test of the validity of the TN formalism/Adam−Gibbs model is to investigate the dependence of the fictive temperature on the thermal history. Integration of eq 4.2 leads to the result

$$\int_{T_0}^{T_{f'}} \mathrm{d}T_f = \int_{T_0}^{T_1} C_p^N \, \mathrm{d}T \qquad (5.2)$$

where T_0 is a temperature well above and T_1 well below the glass transition temperature, T_g. The upper integration limit on the left-hand side is given by the final value of the fictive temperature, $T_{f'}$. The graphic representation of eq 5.2 is shown in Figure 11. Values for $T_{f'}$ from experiment along with the calculated results of the DSC model and T_g values defined by C_p^N are compiled in Table 5.

(c) Dielectric Relaxation. Normalized imaginary parts ϵ'' for A-095.11 at different temperatures are plotted in Figure 12. The origin of the increase in loss at high frequency is unclear, however, it was observed in all measurements with a peak position ($\approx 5 \times 10^6$ Hz) independent of temperature. The relaxation times derived from dielectric loss curves are depicted in Figure 13. They clearly show a FTH dependence above the glass transition in accordance with eq 3.18. The FTH and WLF parameters are given in Table 6 together with low- and high-frequency dielectric constants ϵ_0 and ϵ_∞. For comparison, the refractive indices $n^2 = \epsilon_\infty$ are also included.[5] Note also the difference to the parameters obtained from DSC measurement (Table 4) and the discussion in section VI.

(d) Decay of the SHG Intensity. Normalized SHG decay data for A-148.02 together with KWW fits are given in Figure 14. Measured data were processed as described in section IVc. Curves at 80 and 100 °C are from corona-poled films. All others originate from electrode poled films. The difference between these two poling procedures becomes significant for temperatures $T > T_g - 20$ K. Relaxation times recorded with the first technique are increased, most probably due to residual charge carriers, by up to 2 orders of magnitude.

At low temperatures, decay times become large compared to the available beam time. Extrapolations where the fitted decay time τ_{or} exceeds the actual measured time period by more than 3 orders of magnitude are very uncertain and not included in the scaling graph, Figure 15, where decay times for all the polymers are shown. Filled points belong to corona-poled samples, open points to electrode-poled samples. Points with error bars are averaged values from at least three different films. Similar uncertainties can be expected for all other SHG decay times.

(e) Scaling of Relaxation Times. Within experimental error, a good matching of relaxation times is observed for all polymers in the scaling graph, Figure 15. Results from dielectric measurements are also seen together with the corresponding FTH fit for A-095.11 (dashed line). As both of the WLF parameters for all of these polymers are approximately the same, the dielectric relaxation times fall onto nearly the same line. However, the SHG results clearly demonstrated that the FTH equation cannot describe the relaxation behavior below T_g.

Table 5. $T_f^{graphic}$, T_f^{calc}, and T_g($C_p^N = 0.5$) in K for Different Thermal Histories

cooling/heating rate (K/min)	A-095.11			A-097.07			A-148.02		
	$T_f^{graphic}$	T_f^{calc}	T_g	$T_f^{graphic}$	T_f^{calc}	T_g	$T_f^{graphic}$	T_f^{calc}	T_g
−40/20	408.9	408.4	410.7				442.8	442.8	445.2
−20/20	407.3	406.5	409.1				441.9	441.8	444.6
−10/20	406.8	406.1	409.1	422.2	421.7	423.7	440.7	440.7	444.5
−5/20	406.8	406.0	410.0	420.5	420.0	422.4	439.6	439.7	444.3
−2.5/20	405.0	404.1	409.9	420.3	419.9	422.6	438.4	438.5	444.3
−1.25/20	403.5	402.7	409.9	418.7	418.3	422.6	436.6	436.6	443.5
−0.62/20	404.2	403.2	411.6	418.4	418.0	422.0	435.9	436.2	444.9
−0.31/20	405.1	404.2	413.0				436.0	436.3	446.6

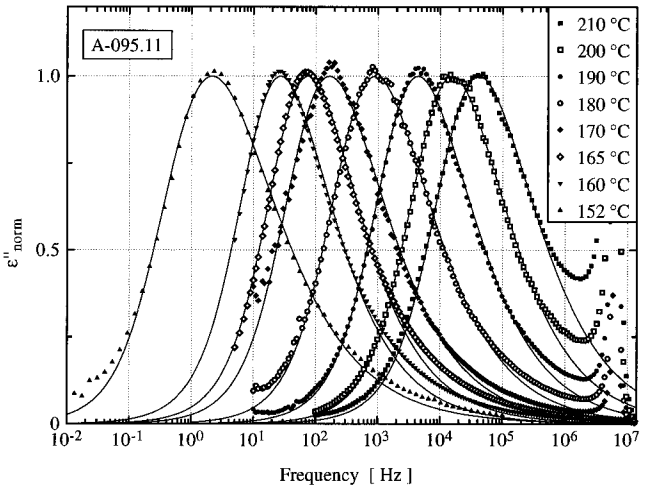

Figure 12. Normalized dielectric loss ϵ'' frequency dependence of A-095.11. Solid lines give the Laplace transform of the Kohlrausch−Williams−Watts (KWW) function.

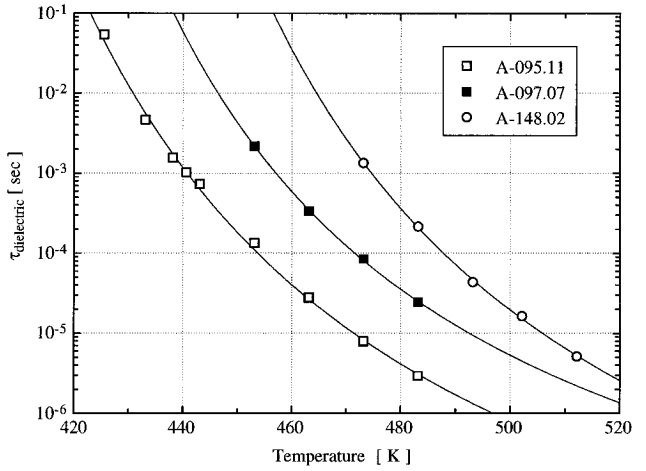

Figure 13. Dielectric loss relaxation times for the three polymers studied in this work. Solid lines are according to the Fulcher−Tammann−Hesse (FTH) equation.

To describe the global relaxation behavior, we used the TN model with parameter values taken from Table 6 using the WLF fits to the dielectric data from temperatures above T_g. Rewriting eq 3.16 in terms of the WLF parameters gives

$$\log R_\tau^g = -C_1^g + \frac{C_1^g C_2^g}{T(1 - T_2/T_f)} \qquad (5.3)$$

where T_f is calculated by eq 3.6. With a cooling rate of 5 K/min (corresponding to the cooling rate used in SHG relaxation experiments), we calculate (via eq 5.3) relaxation times as indicated by the solid line in the scaling graph. The only adjustable parameter $b = 0.21$ was determined by a least squares fit (on a logarithmic time scale) to all the data from electrode-poled films. This value is similar to what is calculated from eq 5.1 (parameter values $b = 0.1$, $T_2 = 356$ K, $T_{f'} = 394$ K) and close to b from SHG relaxation at the lowest temperatures. The TN/WLF analysis displays Arrhenius behavior for temperatures $T < T_g - 100$ K with an activation energy of 1.3×10^5 J/mol, which is lower by almost a factor of 2 as previously published[5] because only corona-poled films were taken into account in the earlier analysis.

VI. Discussion

If eq 3.7 is normalized with respect to a reference relaxation time τ_{ref} above T_g, the fictive temperature $T_f = T$, and one obtains

$$\ln \frac{\tau}{\tau_{ref}} = \ln \frac{A}{\tau_{ref}} + \frac{B}{T - T_2} \qquad (6.1)$$

which is the normalized FTH equation. With the recognition that eq 6.1 has the same functional form as the WLF equation, eq 3.18, it is readily apparent that they must be related by eq 3.15, which defines the preexponential factor A. However, the results of section IIIc indicates that there is a correlation of the Adam−Gibbs DSC parameters such that $\tau_{ref} \approx \tau_g$. And although eq 3.15 introduces two new variables (namely T_g and τ_g) to be determined in the TN formalism using eq 3.7, Table 2 indicates that their values can be restricted to a fairly narrow range. Experimentally, the glass transition temperature can be fairly accurately determined, with a corresponding relaxation time of approximately 10−100 s. Thus, the number of fitted parameters in the TN formalism is reduced to essentially three (B, T_2, and b) instead of the previous four (A, B, T_2, and b). This is a considerable aid in fitting DSC data. However, the precise determination of B and T_2 from DSC results is still rather difficult as there seems to be a fairly wide range of values of these parameters that give approximately similar fits to the the DSC data.

More commonly, values of B and T_2 are determined from relaxation studies above the glass transition and fitting the corresponding relaxation times to the FTH or WLF equation. In fact, it is possible to describe DSC measurements in fair agreement with theory by using eqs 3.5, 3.6, and 5.3 and the TN formalism as shown in Figure 16, and by making use of the WLF parameters C_1^g and C_2^g from the dielectric loss data above T_g. However, as has been previously observed in the analysis of polystyrene DSC data by Hodge,[57] optimal DSC parameters are invariably found to have much lower T_2 values than would be indicated from the WLF analysis of dielectric or mechanical relaxation data above T_g. And although the parameters describing the different relaxation and recovery processes need not be the same, these low T_2 values are related to the low preexponential factors observed in other results.[19,58] Our results are also in agreement with other work that indicates that the TN procedure is unable to reproduce

Table 6. Fulcher−Tammann−Hesse (FTH) Parameters from Dielectric Relaxations Together with Low- and High-Frequency Dielectric Constants and Refractive Indices Squared

polymer	C_1^g	C_2^g (K)	B (10^3 K)	T_g (K)	T_2 (K)	log(τ_g (s)/s)	ϵ_0	ϵ_∞	$n^2_{\omega\to 0}$
A-095.11	12 ± 3	54 ± 9	1.5 ± 0.3	410	356 ± 9	1.3 ± 0.6	13 ± 1	3.4 ± 0.4	2.7
A-097.07	12 ± 2	45 ± 7	1.2 ± 0.2	422	377 ± 7	2.1 ± 0.3	10.3 ± 0.3	2.5 ± 0.4	2.7
A-148.02	11 ± 4	56 ± 15	1.5 ± 0.4	445	389 ± 15	1.0 ± 0.3	13.3 ± 0.2	3.6 ± 0.2	2.7

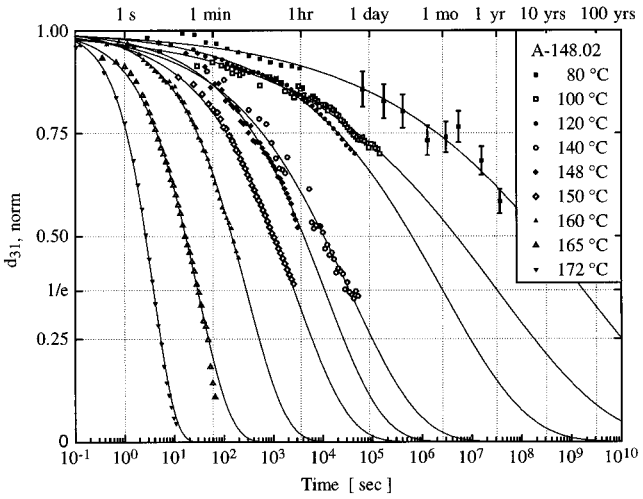

Figure 14. Normalized SHG relaxation times for the polyimide side-chain polymer A-148.02 fitted to the Kohlrausch−Williams−Watts (KWW) function.

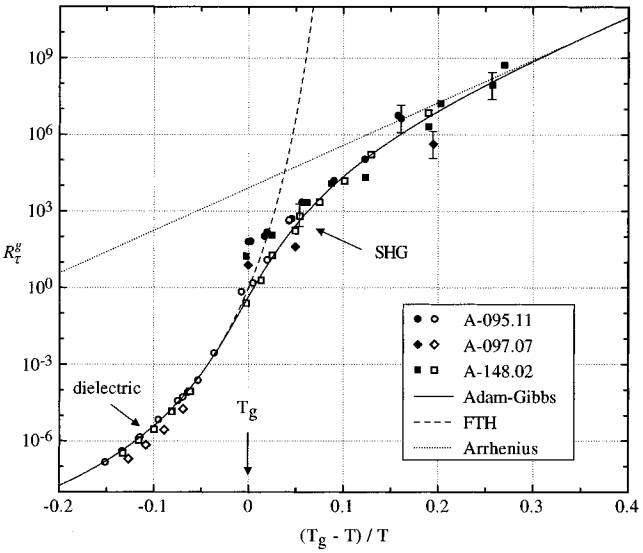

Figure 15. Temperature scaling of normalized dielectric loss and SHG relaxation times with respect to the scaling variable $(T_g - T)/T$ of the three polymers studied in this work. Open points refer to electrode-poled films, filled points to corona poled films. Points with error bars are averaged values from at least three different films. All points below T_g are form SHG relaxations whereas points above T_g originate from dielectric relaxation measurements. The influence of the structure on relaxation becomes obvious slightly above T_g, where the Adam−Gibbs line deviates form the Fulcher−Tammann−Hesse (FTH) line. All curves were calculated with the Fulcher−Tammann−Hesse parameters for the polyimide side-chain polymer A095.11, although the parameters for A-097.07 and A-148.02 would also have been convenient due to the expected scaling. The FTH line was calculated with eq 3.17, whereas eq 3.16 with the procedure outlined in the text for the determination of T_f was used for the Adam−Gibbs line. Note that the predicted Arrhenius behavior is observed only at temperatures well below T_g.

all the details of the observed DSC phenomena.[7,20,27] For example, it is not possible to use the same nonexponentiality parameter b for all thermal histories and obtain optimized fits to the DSC data. These results appear

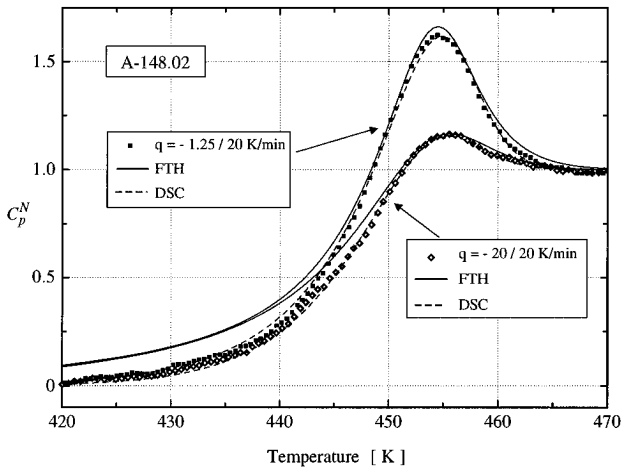

Figure 16. Comparison of DSC traces calculated with the Tool−Narayanaswamy formalism using best fit (DSC) parameter sets and Fulcher−Tammann−Hesse (FTH) parameters from dielectric relaxation.

Table 7. Comparison of the Evaluation of the Same DSC Traces Using either Fulcher−Tammann−Hesse (FTH) or DSC Parameters for Polyimide Side-Chain Polymer A-148.02

data	parameter set	q (K/min)	B (10^3 K)	T_2 (K)	T_g (K)	τ_g (s)	b
dielectric	FTH	NA	1.46	389	444	15	0.46−0.64
DSC	FTH	−20/20	1.46	389	445	50	0.40
DSC	FTH	−1.25/20	1.46	389	444	62	0.32
DSC	DSC	−20/20	22.6	189	445	25	0.47
DSC	DSC	−1.25/20	31.3	137	444	62	0.53

to indicate a failure in the manner in which nonexponentiality or nonlinearity is treated by the TN method. It seems likely that it may be necessary to develop a model of the glass transition that incorporates the fact that real materials are thermorheologically complex in order to accurately model their enthalpic response.[59]

However, as seen in Figure 15, the dielectric and SHG relaxation results of the NLO polymers investigated in this work are well modeled using the TN formalism incorporating the WLF parameterization. An intuitive understanding of these results are perhaps best clarified through the use of free-volume concepts. The fractional free volume f is described in terms of the relative difference of the total volume, v, and the occupied volume of the molecules, v_0:

$$f = \frac{v - v_0}{v} = \frac{v_f}{v} \approx f_g + \alpha_f(T - T_g) \qquad (6.2)$$

where f_g is the fractional free volume at the glass transition temperature and the coefficient of thermal expansion is denoted by α_f. The WLF parameters C_1^g and C_2^g can then be expressed in terms of free-volume parameters as follows:[6,37]

$$C_1^g = \frac{1}{2.303}\frac{\tilde{b}}{f_g} \qquad C_2^g = \frac{f_g}{\alpha_f} \qquad (6.3)$$

where $\tilde{b}$ is an empirical material constant. Thus, the slope of our "universal" relation (eq 3.20) describing

relaxation below T_g is inversely proportional to the fractional free volume available to the chromophores at the glass transition temperature. Although the WLF parameter C_1^g is known to be polymer dependent, values of $f_g/\tilde{b}$ determined by mechanical measurements vary over a relatively small range from about 0.013 to 0.034.[6] This implies that the values of C_1^g range from approximately 13 to 34. From SHG decay measurements on a variety of polymeric systems, we find that the slope of eq 3.20 (given by C_1^g) falls near the lower end of this range. Thus, for NLO polymers that incorporate chromophores of approximately the same size we would expect scaling in a plot of relaxation times vs $(T_g - T)/T$ to be "universal" in the sense that the fractional free volume probed by the chromophores should be nearly the same.

The algorithm developed in this work, based on eq 5.3, enables us to calculate the relaxation times describing the orientational properties of NLO polymers as a function of both temperature and processing conditions. As an example, we can apply these results to a hypothetical EO device utilizing a NLO polymer as the active material. In order to limit the decrease in the EO coefficient to less than 5% of the initial value over a device lifetime of ≈5 years and operation at 80 °C, a glass transition temperature of about 270 °C is needed ($\tau = 2.2 \times 10^{14}$ s, $(T_g - T)/T = 0.53$, $b = 0.21$). The polymer A-148.02 would retain only 56% of the initial nonlinearity under these conditions. NLO polymers having glass transition temperatures in this range and higher are under current research development.[60]

Other authors[61−64] have given an alternative description of the temperature dependence of SHG relaxation times below T_g in analogy with the FTH equation. They proposed the following expression to correlate their data describing the temperature dependence of the SHG decay times, $\tau(T)$, for a variety of guest−host NLO polymer matrices:

$$\tau(T) = A' \exp\left(\frac{-B'}{T_0' - T}\right) \qquad (6.4)$$

with, however, $T_0' \approx T_g + (50 \pm 10)$ °C. Data points from several guest−host systems lie more or less on the same straight line in the corresponding scaling plot. In subsequent measurements on NLO poly(methyl methacrylate) side-chain polymers, strong deviations from this relation were found for temperatures below $T_g - 50$ °C.[63] The use of eq 6.4, however, has no clear interpretation in terms of the WLF theory, in contrast to the results presented in this paper where the relaxation below T_g is dependent on the fractional free volume probed by the chromophores at T_g, eqs 3.20 and 6.3.

VII. Conclusions

An improved version of the TN formalism for calculating relaxation and recovery processes in glasses has been presented. Using the relationship for the preexponential factor given by eq 3.15, we find that the relaxation time probed by DSC, dielectric relaxation, and SHG relaxation has a "universal" value of 10−100 s at T_g for very different types of glass formers. The DSC results also indicate that implementations of the TN formalism by some other authors are not equivalent, as indicated by the different results for some glasses (see Table 2). However, the results presented here are in agreement with previous experimental work, indicating that the TN procedure adequately describes most of, but not the complete behavior of enthalpic relaxation and recovery processes for all thermal histories.

Relaxation processes in NLO-active modified polyimide polymers with side-chain azo chromophores having glass transition temperatures in the range of $140 < T_g < 170$ °C have been studied. We have shown that it is possible to model the relaxational behavior of NLO chromophores both above and below the glass transition over more than 15 orders of magnitude in time using the TN procedure incorporating the appropriate WLF parameters for the NLO polymer. This leads to a scaling prediction for relaxation times in the glassy state with scaling parameter $(T_g - T)/T$. The TN procedure including our minor modification provides an excellent framework for the nonlinear extension of the liquid-state relaxation behavior through the glass transition as suggested by the consistency between observed and calculated relaxation times below the glass transition. Prediction of the relaxation times as a function of both temperature and processing conditions (cooling rates, annealing times and temperatures, etc.) can then be made. Work in progress on this aspect of NLO polymers will be reported at a later date.

Furthermore, our interpretation leads to the prediction that SHG decay below T_g should be Arrhenius-like if the chromophore orientation is entirely coupled to the primary or α-relaxation processes. We find that this prediction is fulfilled to a much greater extent by side-chain NLO polymers than for guest−host polymer systems.[5] Guest−host NLO matrices appear to have a limited relative thermal stability and deviate significantly from Arrhenius behavior at temperatures far below the glass transition.

Acknowledgment. We thank H. Scherrer for the deposition of the gold electrodes used for the dielectric measurements and S. Vartanen for the use of the Zehnder IM5 impedance analyzer. D. Jundt provided assistance in the initial setup of the HP 4129A LF impedance analyzer.

Appendix: Computational Notes

The computation of enthalpic relaxation processes as measured by DSC was done by numerical integration of eq 3.6. The evolution of the fictive temperature was calculated via a summation procedure as described by Hodge and Berens,[28] with the exception that the time response was calculated using eqs 3.7 and 3.15. Continuous heating and/or cooling at a rate q was described by a series of temperature steps, ΔT, followed by isothermal holds of duration $\Delta t = \Delta T/q$. To ensure linearity, the magnitude of ΔT was typically chosen to be 0.2−0.5 K, as temperature steps of $\Delta T = 0.1$ K were found to give no further changes in the calculated enthalpic response. Parameter optimization was accomplished via a Levenson−Marquardt fitting algorithm available on proFit (published by Cherwell Scientific).

The frequency dependence of the dielectric relaxation data was calculated and optimized using eqs 3.26 to 3.28 and using the same proFit fitting algorithm. Using these equations, we obtain approximately six digit accuracy for z in the range $10^{-4} < z < 10^4$, which is sufficient for fitting all of our dielectric relaxation data. Parts a and b of Figure 17 show the comparison of our calculated values of $z\,Q(z)$ for $b = 0.1$ and 0.5 with the tabulated values of Dishon et al.,[33] which are reported to be accurate to six digits in floating point. These

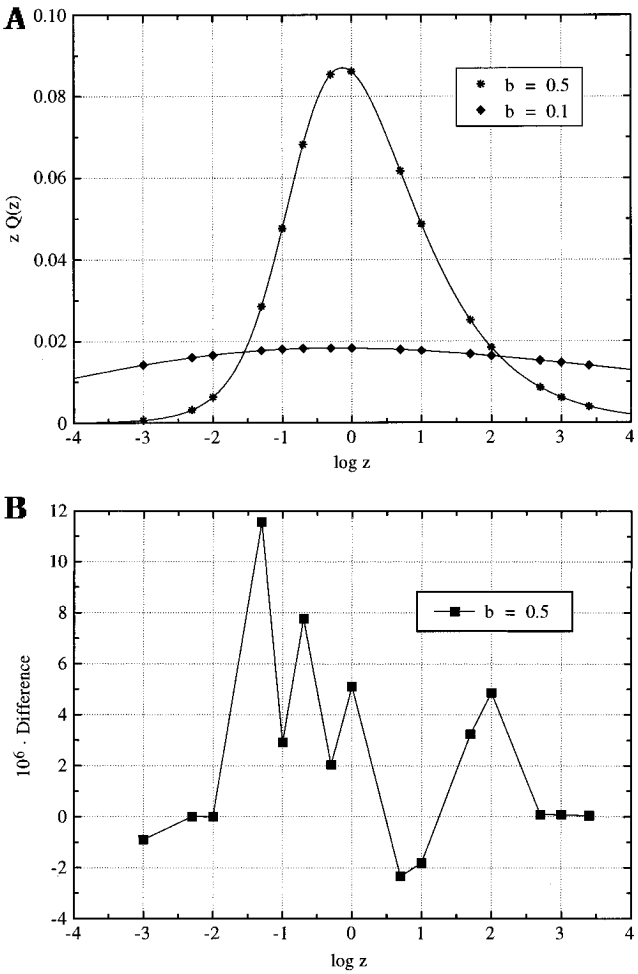

Figure 17. (a) Comparison of calculated values of $zQ(z)$ as used for fitting dielectric loss data with the tabulated values of Dishon et al.[33] (b) Comparison of $10^6 \times$ difference of the calculated values of $zQ(z)$ as used for fitting dielectric loss data with the tabulated values of Dishon et al.[33]

results appear to be similar to those obtained by other methods.[65]

References and Notes

(1) Meredith, G. R.; Dusen, J. G. V.; Williams, D. J. *Macromolecules* **1982**, *15*, 1385−1389.
(2) Singer, K. D.; Sohn, J. E.; Lalama, S. J. *Appl. Phys. Lett.* **1986**, *49*, 248−250.
(3) McKenna, G. B. In *Comprehensive Polymer Science—2*; Allen, G., Ed.; Pergamon Press: New York, 1989; p 311.
(4) Ahlheim, M.; Lehr, F. *Makromol. Chem.* **1994**, *195*, 361−373.
(5) Prêtre, P.; Kaatz, P.; Bohren, A.; Günter, P.; Zysset, B.; Ahlheim, M.; Stähelin, M.; Lehr, F. *Macromolecules* **1994**, *27*, 5476−5486.
(6) Ferry, J. D. *Viscoelastic Properties of Polymers*; J. Wiley & Sons: New York, 1980.
(7) Hodge, I. M. *J. Non-Cryst. Solids* **1994**, *169*, 211−266.
(8) Kovacs, A. J.; Hutchinson, J. M.; Aklonis, J. J. In *The Structure of Non-Crystalline Materials*; Gaskell, P. H., Ed.; Taylor and Francis: London, 1977; p 153.
(9) Di Marzio, E. A.; Gibbs, J. H. *J. Chem. Phys.* **1958**, *28*, 373.
(10) Adam, G.; Gibbs, J. H. *J. Chem. Phys.* **1965**, *43*, 139−145.
(11) Scherer, G. W. *J. Am. Ceram. Soc.* **1984**, *67*, 504.
(12) Kauzmann, W. *Chem. Rev.* **1948**, *43*, 219.
(13) Tool, A. Q. *J. Am. Ceram. Soc.* **1946**, *29*, 240.
(14) Narayanaswamy, O. S. *J. Am. Ceram. Soc.* **1971**, *54*, 471.
(15) Moynihan, C. T.; Macedo, P. B.; Montrose, C. J.; Gupta, P. K.; DeBolt, M. A.; Dill, J. F.; Drake, P. W.; Easteal, A. J.; Elterman, P. B.; Moeller, R. P.; Sasabe, H.; Wilder, J. A. *Ann. N.Y. Acad. Sci.* **1976**, *279*, 15.
(16) DeBolt, M. A.; Easteal, A. J.; Macedo, P. B.; Moynihan, C. T. *J. Am. Ceram. Soc.* **1976**, *59*, 16−21.
(17) Hodge, I. M. *Macromolecules* **1983**, *16*, 898−902.
(18) Hodge, I. M. *J. Non-Cryst. Solids* **1991**, *131*−133, 435.
(19) Hodge, I. M. *Macromolecules* **1987**, *20*, 2897−2908.
(20) Moynihan, C. T.; Crichton, S. N.; Opalka, S. M. *J. Non-Cryst. Solids* **1991**, *131*−133, 420.
(21) Kohlrausch, R. *Pogg. Ann. Phys.* **1854**, *91*, 179−214.
(22) Williams, G.; Watts, D. C. *Trans. Faraday Soc.* **1970**, *66*, 80.
(23) Beckmann, P. A. *Phys. Rep.* **1988**, *171*, 85−128.
(24) Pollard, H. *Bull. Am. Math. Soc.* **1946**, *52*, 908−910.
(25) Lindsay, C. P.; Patterson, G. D. *J. Chem. Phys.* **1980**, *73*, 3348.
(26) Moynihan, C. T.; Boesch, L. P.; Laberge, N. L. *Phys. Chem. Glasses* **1973**, *14*, 122−125.
(27) O'Reilly, J. M.; Hodge, I. M. *J. Non-Cryst. Solids* **1991**, *131*−133, 451.
(28) Hodge, I. M.; Berens, A. R. *Macromolecules* **1982**, *15*, 762.
(29) Rekhson, S. M. *J. Non-Cryst. Solids* **1986**, *84*, 68−85.
(30) Scherer, G. W. *J. Am. Ceram. Soc.* **1986**, *69*, 374.
(31) Montroll, E. W.; Bendler, J. T. *J. Stat. Phys.* **1984**, *34*, 129−162.
(32) Weiss, G. H.; Bendler, J. T.; Dishon, M. *J. Chem. Phys.* **1985**, *83*, 1424−1427.
(33) Dishon, M.; Weiss, G. H.; Bendler, J. T. *J. Res. Natl. Bur. Stand.* **1985**, *90*, 27−32.
(34) Macdonald, J. R.; Hurt, R. L. *J. Chem. Phys.* **1986**, *84*, 496−502.
(35) Gómez Ribelles, J. L.; Ribes Greus, A.; Calleja, D. *Polymer* **1990**, *31*, 223−230.
(36) Crichton, S. N.; Moynihan, C. T. *J. Non-Cryst. Solids* **1988**, *102*, 222−227.
(37) Kovacs, A. J. *Fortsch. Hochpolym.-Fortsch.* **1963**, *3*, 394−507.
(38) Flynn, J. F. *Thermochim. Acta* **1974**, *8*, 69−81.
(39) Moynihan, C. T.; Easteal, A. J.; DeBolt, M. A.; Tucker, J. *J. Am. Ceram. Soc.* **1976**, *59*, 12−16.
(40) Blythe, A. R. *Electrical Properties of Polymers*; Cambridge University Press: Cambridge, 1979.
(41) Böttcher, C. J. F.;Bordewijk, P. *Theory of Electric Polarization*; Elsevier: Amsterdam, 1978.
(42) Williams, G. *Chem. Rev.* **1972**, *72*, 55−69.
(43) Williams, G. In *Comprehensive Polymer Science—2*; Allen, G., Ed.; Pergamon Press: New York, 1989; p 311.
(44) Cauchy, A. *C. R. Acad. Sci.* **1853**, *37*, 202.
(45) Wintner, A. *Duke Math. J.* **1941**, *8*, 678−681.
(46) Williams, G.; Watts, D. C.; Dev, S. B.; North, A. M. *Trans. Faraday Soc.* **1971**, *67*, 1323.
(47) Chung, S. H.; Stevens, J. R. *Am. J. Phys.* **1991**, *59*, 1024−1030.
(48) Weiss, G. H.; Dishon, M.; Long, A. M.; Bendler, J. T.; Jones, A. A.; Inglefield, P. T.; Bandis, A. *Polymer* **1994**, *35*, 1880−1883.
(49) Koizumi, N.; Kita, Y. *Bull. Inst. Chem. Res., Kyoto Univ.* **1978**, *56*, 300.
(50) Meredith, G. R.; Vandusen, J. G.; Williams, D. J. In *Nonlinear Optical Properties of Organic and Polymeric Materials*; Williams, D. J., Ed.; ACS Symposium Series 233; American Chemical Society: Washington, DC, 1983; pp 109−133.
(51) Wu, J. W. *J. Opt. Soc. Am.* **1991**, *B8*, 142−152.
(52) Howell, F. S.; Bose, R. A.; Macedo, P. B.; Moynihan, C. T. *J. Phys. Chem.* **1974**, *78*, 639−648.
(53) Köhler, W.; Robello, D. R.; Dao, P. T.; Willand, C. S.; Williams, D. J. *J. Chem. Phys.* **1990**, *93*, 9157.
(54) Moynihan, C. T. *J. Non-Cryst. Solids* **1994**, *172*−174, 1395−1407.
(55) Dhinojwala, A.; Wong, G. K.; Torkelson, J. M. *J. Opt. Soc. Am.* **1994**, *B11*, 1549−1554.
(56) Dhinojwala, A.; Wong, G. K.; Torkelson, J. M. *J. Chem. Phys.* **1994**, *100*, 6046−6054.
(57) Hodge, I. M. *Macromolecules* **1986**, *19*, 936.
(58) Sales, B. C. *J. Non-Cryst. Solids* **1990**, *119*, 136−150.
(59) Ducroux, J. P.; Rekhson, S. M.; Merat, F. L. *J. Non-Cryst. Solids* **1994**, *172*−174, 541−553.
(60) Miller, R. D.; Burland, D. M.; Jurich, M.; Lee, V. Y.; Moylan, C. R.; Thackara, J. I.; Tweig, R. J.; Verbiest, T.; Volksen, W. *Macromolecules* **1995**, *28*, 4970−4974.
(61) Stähelin, M.; Burland, D. M.; Ebert, M.; Miller, R. D.; Smith, B. A.; Twieg, R. J.; Volksen, W.; Walsh, C. A. *Appl. Phys. Lett.* **1992**, *61*, 1626.
(62) Stähelin, M.; Walsh, C. A.; Burland, D. M.; Miller, R. D.; Twieg, R. J.; Volksen, W. *J. Appl. Phys.* **1993**, *73*, 8471−8479.
(63) Walsh, C. A.; Burland, D. M.; Lee, V. Y.; Miller, R. D.; Smith, B. A.; Twieg, R. J.; Volksen, W. *Macromolecules* **1993**, *26*, 3720−3722.
(64) Burland, D. M.; Miller, R. D.; Walsh, C. A. *Chem. Rev.* **1994**, *94*, 31−75.
(65) Havriliak, S.; Havriliak, S. J. *Polymer* **1995**, *36*, 2675−2680.

MA9509927